Variation of the Ru moment in the $Ca_{0.3}Sr_{0.7}Ru_{1-x}Mn_xO_3$ system

2010 J. Phys.: Condens. Matter 22 145601

(http://iopscience.iop.org/0953-8984/22/14/145601)

J. Phys.: Condens. Matter **22** (2010) 145601 (8pp) doi:10.1088/0953-8984/22/14/145601

Variation of the Ru moment in the $Ca_{0.3}Sr_{0.7}Ru_{1-x}Mn_xO_3$ system

S Mizusaki[1], M Naito[1], T Taniguchi[1], Y Nagata[1], M Itou[2], Y Sakurai[2], Y Noro[3], T C Ozawa[4] and H Samata[5]

[1] College of Science and Engineering, Aoyama Gakuin University, Sagamihara, Kanagawa 157-8572, Japan
[2] Japan Synchrotron Radiation Research Institute (JASRI/SPring-8), Sayo, Hyogo 679-5198, Japan
[3] Kawazoe Frontier Technologies, Co. Ltd, Sakae, Yokohama, Kanagawa 931-113, Japan
[4] Nanoscale Materials Center, National Institute for Materials Science, Namiki, Tsukuba, Ibaraki 305-0044, Japan
[5] Faculty of Maritime Sciences, Kobe University, Higashinada, Kobe, Hyogo 658-0022, Japan

Received 22 October 2009, in final form 16 February 2010
Published 17 March 2010
Online at stacks.iop.org/JPhysCM/22/145601

Abstract
The variation of the magnetic moment on Ru and Mn atoms in the $Ca_{0.3}Sr_{0.7}Ru_{1-x}Mn_xO_3$ system was investigated by the magnetic Compton scattering technique using synchrotron radiation. The $Ca_{0.3}Sr_{0.7}Ru_{1-x}Mn_xO_3$ system has ferrimagnetism with an antiferromagnetic coupling between Ru and Mn, and the dominant magnetic component changes from ferromagnetic Ru to ferromagnetic Mn at $x \sim 0.25$ as the Mn substitution proceeds. The mechanism for the change in the magnetism of $Ca_{0.3}Sr_{0.7}Ru_{1-x}Mn_xO_3$ is discussed.

1. Introduction

Perovskite-type ruthenium oxides have attracted much attention because of their interesting magnetic and transport properties. Among the ruthenium oxides, the ferromagnet $SrRuO_3$ ($T_C = 160$ K) and paramagnet $CaRuO_3$ are well known to be isostructural itinerant oxides [1–8]. It was reported that ferromagnetism is induced in $CaRuO_3$ when a very small amount of magnetic or nonmagnetic ions are substituted to the Ru site [1–3, 9]. It is also well recognized that Sr substitution to the Ca sites [1–8] changes the magnetic state of Ru^{4+} ions from paramagnetic to ferromagnetic. These facts clearly show that $CaRuO_3$ is a material on the border between paramagnetism and ferromagnetism.

In particular, Mn substitution for $CaRuO_3$ causes ferromagnetism for a relatively large substitution level ($\geqslant 0.1$) [10–17]. The study of the $CaRu_{1-x}Mn_xO_3$ system [10–17] revealed the existence of a correlation between Ru and Mn ions and the fact that the magnetic states of the Ru ion change from paramagnetic to ferromagnetic by Mn substitution. It was also suggested that the ground state of this system is established by the mixed valence states of Ru and Mn ions [14], and the magnetic inhomogeneity consisting of the paramagnetic and ferrimagnetic ground states or antiferromagnetic and ferrimagnetic ground states was revealed by the magnetic Compton scattering experiment [20, 21].

In a previous paper [18], we showed that $Ca_{0.5}Sr_{0.5}Ru_{0.4}Mn_{0.6}O_3$ in the $Ca_{1-y}Sr_yRu_{1-x}Mn_xO_3$ system had a higher Curie temperature of 275 K. This system seems to be a typical material in which new magnetism, which is induced by a closed relationship between the lattice deformation and various exchange interactions, will occur. However, in the $SrRu_{1-x}Mn_xO_3$ system, the ferromagnetism of $SrRuO_3$ is suppressed by Mn substitution [22, 23]. This suggests that the Mn substitution suppresses the itinerant nature of Ru^{4+} (t_{2g}) in $SrRuO_3$ and a localized state is realized in $SrRu_{1-x}Mn_xO_3$ for larger substitution.

In the present study, a magnetic Compton scattering experiment was conducted for a polycrystalline $Ca_{0.3}Sr_{0.7}Ru_{1-x}Mn_xO_3$ system to reveal the magnetic ground state. In this paper, the mechanism of the magnetism is discussed from the viewpoint of the relationship between the result of the magnetic Compton scattering experiment and the results of the crystallographic, magnetic and transport properties.

2. Experimental details

The preparation method of polycrystalline $Ca_{0.3}Sr_{0.7}Ru_{1-x}Mn_xO_3$ was the same as that described previously [14, 18]. The chemical composition and homogeneity were characterized by electron-probe microanalysis (EPMA) using wavelength-dispersive spectrometers. The crystal structure was character-

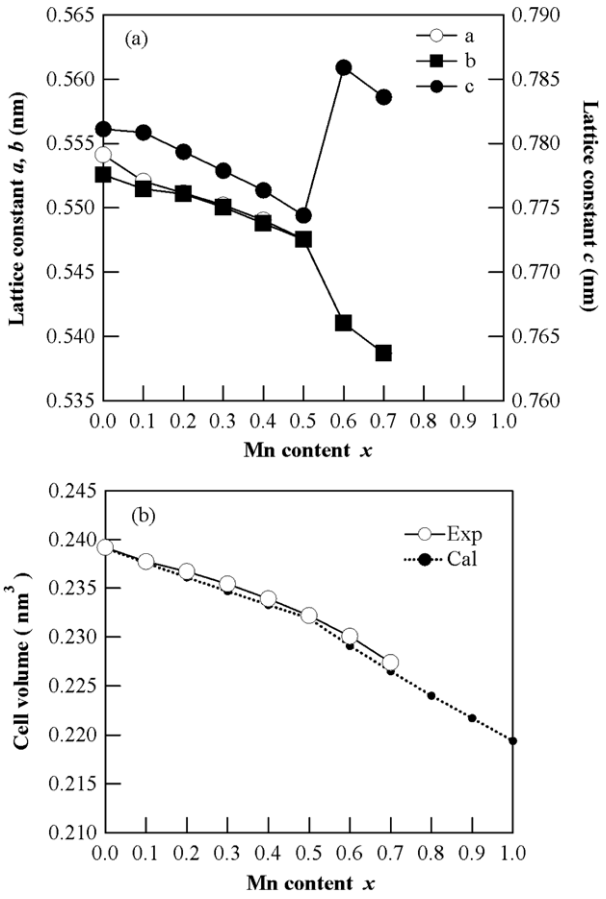

Figure 1. (a) Mn content dependence of lattice constant and (b) cell volume of $Ca_{0.3}Sr_{0.7}Ru_{1-x}Mn_xO_3$ at room temperature with the calculated curves from the estimated ion rates.

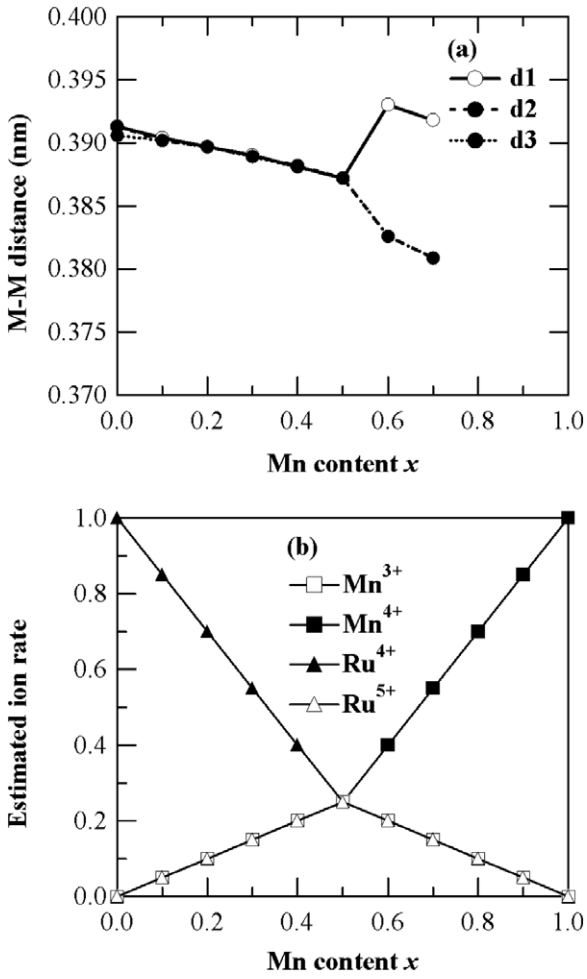

Figure 2. The analysis results of the XRD result at room temperature. (a) The distance between the B site ions with respect to the Mn content. (b) The estimated ion rates from the experimental cell volume. The parameters $d1$, $d2$ and $d3$ correspond to the distance to the neighboring atoms along the three-dimensional directions.

ized at room temperature by x-ray powder diffraction (XRD) using Cu Kα radiation and the crystal structure parameters were refined by the Rietveld method. The magnetic properties were characterized using a superconducting quantum interference device (SQUID) magnetometer. The electrical conductivity was measured using a four-probe method at temperatures down to 5 K. Electrical contact was established using gold wire and silver paste. The magnetoresistance was measured under magnetic fields up to 5 T applied parallel to the electric current.

The magnetic Compton profiles and spin moments were measured with a magnetic Compton scattering (MCS) experiment performed at the BL08W beamline of SPring-8. The sample temperature was 10 K and the applied magnetic field was 2.5 T. The overall momentum resolution was 0.57 atomic units (au). The details of the experiment are described in [24–26]. The usual correction procedures were employed, and, after confirming the symmetrical shape of the MCP with respect to zero momentum, the MCPs were folded at zero momentum to increase the effective statistical accuracy.

3. Experimental results

3.1. Crystal properties

The XRD results are summarized in figures 1 and 2. The results of the refinement for the XRD profile for $Ca_{0.3}Sr_{0.7}Ru_{1-x}Mn_xO_3$ ($0 \leqslant x \leqslant 0.7$) showed a single-phase $GdFeO_3$-type orthorhombic perovskite structure of $Pbnm$ for $x \leqslant 0.5$ or of $I4/mcm$ for $0.5 < x$. The sample with $x = 0.8$ has a crystal structure of $P63/mmc$ symmetry under the present synthesis conditions. The analysis of the XRD results shows that the system is crystallographically homogeneous. The results of the Rietveld analysis are shown in figures 1(a) and (b). As shown in figure 1(b), although the cell volume continuously decreases as the Mn content increases, the lattice parameter has a discontinuity at $x = 0.5$. Moreover, the space group of the crystal structure changes from $Pbnm$ to $I4/mcm$ at $x = 0.5$ (see figure 1(a)).

Figure 2(a) displays the distance d between Ru or Mn ions deduced from the refined crystal lattice parameters. The result indicates that the B site ions form a cubic lattice structure between the Mn content of $x = 0.2$ and 0.5. Figure 2(b) summarizes the estimated ion rates for Ru^{4+}, Ru^{5+}, Mn^{4+} and Mn^{3+} ions using the Mn content dependence of the cell volume shown in figure 1(b). Our neutron diffraction and Mössbauer measurements for $CaRu_{0.85}Fe_{0.15}O_3$ revealed that there is no

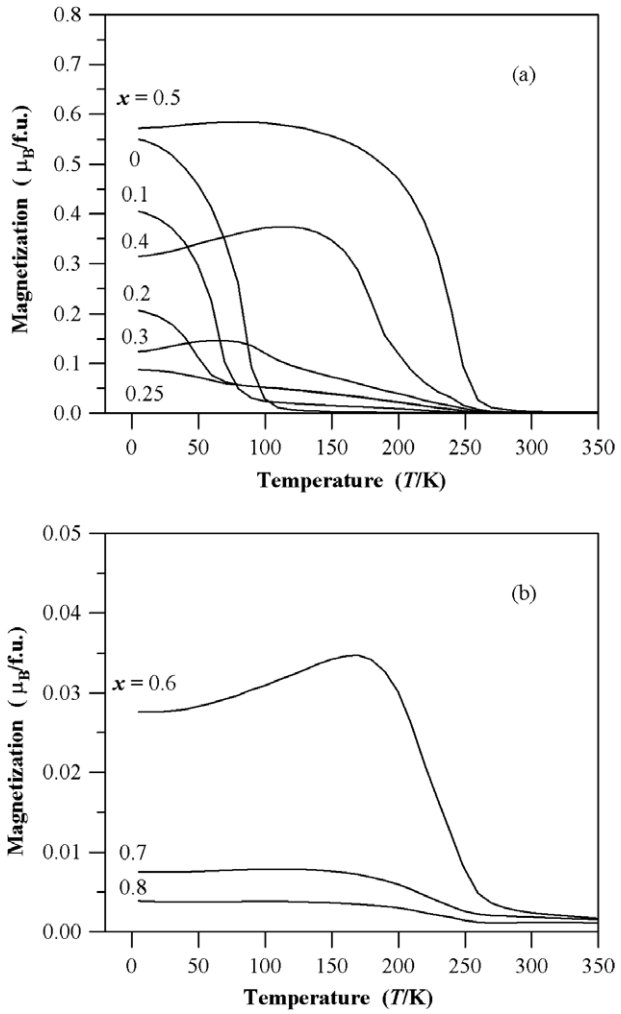

Figure 3. The temperature dependence on magnetization under 1 kOe for $Ca_{0.3}Sr_{0.7}Ru_{1-x}Mn_xO_3$ ((a) $x \leqslant 0.5$, (b) $x > 0.5$).

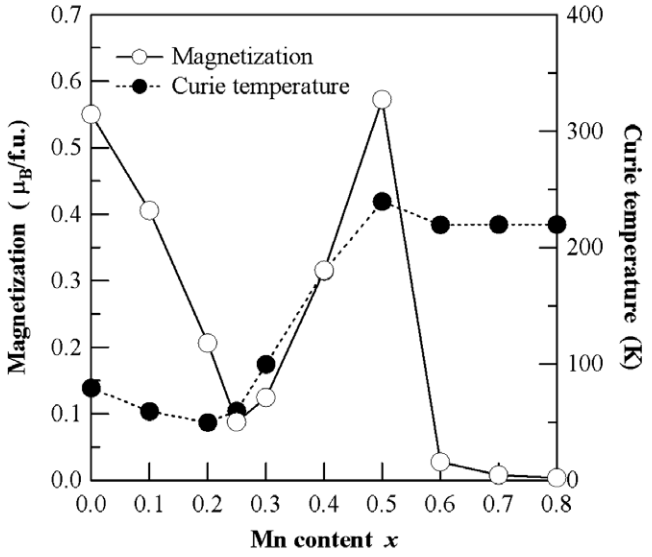

Figure 4. The Mn content dependence on Curie temperature (closed) and the magnetization (open) at 5 K under 1 kOe for $Ca_{0.3}Sr_{0.7}Ru_{1-x}Mn_xO_3$.

oxygen vacancy and that Fe exists as a trivalent ion [19]. Therefore, in the present case, the estimation described in [14] was performed under the assumption of (1) $N^{Mn} = N^{Mn3+} + N^{Mn4+}$, (2) $N^{Mn3+} = N^{Ru5+}$ and (3) $N^{Ru4+} = 1 - N^{Mn} - N^{Ru5+}$, where N^{Mn3+}, N^{Mn4+}, N^{Ru5+} and N^{Ru4+} are the ion rates for each ion, and their sum is 1. The amounts of each ion are $N^{Mn3+} = N^{Mn4+} = N^{Ru5+} = N^{Ru4+} = 0.25$ at $x = 0.5$. It is seen that the experimental cell volume is well represented by the calculated cell volume. These results suggest that the system is in a mixed valence state consisting of Ru^{4+}, Ru^{5+}, Mn^{3+} and Mn^{4+} ions. Furthermore, it is evident that the concentrations of Mn^{3+} and Mn^{4+} are almost the same as long as Ru^{5+} can compensate for the charge imbalance caused by the substitution of Mn^{3+}.

3.2. Magnetic properties

The temperature dependence of magnetization, M, is shown in figure 3. The magnetization shows a ferromagnetic behavior for the samples with $x = 0$ and 0.5 with anomalous temperature dependence. On the other hand, the magnetizations of the samples with $x > 0.5$ become smaller than those of the samples with $x = 0.5$ (see figure 3(b)) with a ferromagnetic-like temperature dependence.

Figure 4 is a summary of the Curie temperature T_C as a function of the Mn content, where T_C was determined by the peak temperature of dM/dT. The variation of T_C and the magnetic moment suggests the existence of a magnetic correlation between Ru and Mn ions. The magnetization at 5 K varied with Mn content and it showed a minimum at $x = 0.25$. In addition, it was also found that the samples for $x = 0.5$–0.6 show a remarkably small magnetization and have a structural transition (as shown in figure 1). On the other hand, T_C yielded from figure 3 changed from 80 K at $x = 0$ to 250 K at $x = 0.5$ through the minimum T_C (50 K) at $x = 0.2$. However, the samples with $x = 0.6$ and 0.8 show T_C with a constant (230 K). The present magnetic and structural results for $x = 0.6$–0.8 suggest that the ferromagnetic transition for $x = 0.6$–0.8 would be caused by the weak ferromagnetic behavior from the antiferromagnetic structure between Mn/Ru moments. Therefore, an antiferromagnetism state would be established in the samples with $x > 0.5$.

3.3. Magnetoresistance effect

Figure 5 shows the temperature dependence of the normalized resistivity $\rho(T)/\rho$ ($T = 270$ K) measured under zero field for samples with $x = 0$–0.7. The behavior of $\rho(T)$ changes from metallic for $x = 0$ to semiconductive with increasing Mn content. The inset of figure 5 shows the resistivity at 10 K as a function of Mn content x. The change observed in the slope $d\rho/dx$ at $x = 0.5$ would be caused by the change in the crystal structure.

The magnetoresistance (MR) effect was characterized for samples with $x = 0.25$, 0.4, 0.5 and 0.7. The MR ratio was defined as $MR = (\rho_H - \rho_0)/\rho_0 \times 100$. Figures 6(a) and (b) show the magnetic field dependence of the MR ratio at 10 K for $x = 0.25$, 0.4, 0.5 and 0.7. Figure 6(a) shows that the MR

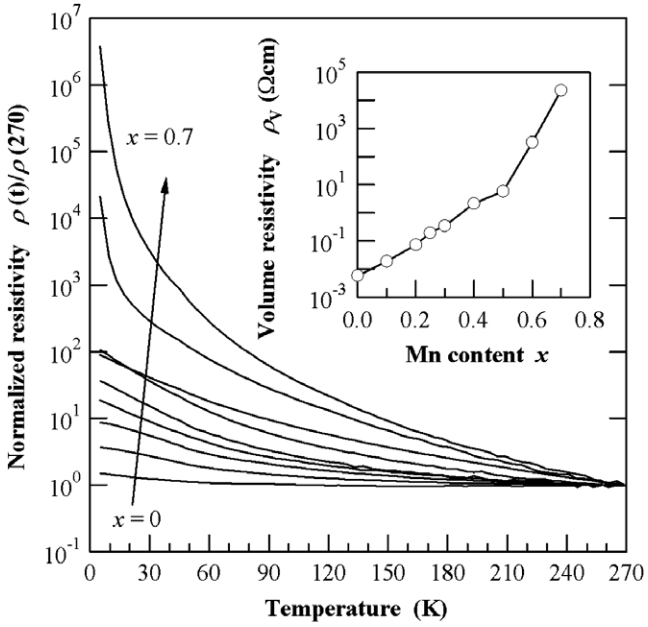

Figure 5. The temperature dependence on electronic resistivity for $Ca_{0.3}Sr_{0.7}Ru_{1-x}Mn_xO_3$ ($0 \leqslant x \leqslant 0.7$). Inset figure shows a volume resistivity for $Ca_{0.3}Sr_{0.7}Ru_{1-x}Mn_xO_3$ ($0 \leqslant x \leqslant 0.7$) at 5 K.

ratio is not saturated even at 5 T. However, no anisotropic MR effect was observed in the measurement of the MR effect along the perpendicular and parallel directions between the current and the applied magnetic field. Figure 6(b) shows that the MR effect was observed in the range of $0.2 < x \leqslant 0.5$ and that an MR effect as large as 30% was observed for a sample with $x = 0.5$ at 10 K. These results indicate that the Mn substitution induces an MR effect. A similar MR effect has been observed for $Ca_{0.3}Sr_{0.7}RuO_3$ (~3%) in the study of $Ca_{1-x}Sr_xRuO_3$ [8].

3.4. Phase diagram for this system

The experimental results obtained above are summarized in figure 7 to reveal the relation between the properties and Mn content. The results show that a magnetic structure transition occurs above $x = 0.5$ associated with a crystal structure transition. The Mn content seems to play a key role in the change of physical properties. Based on this experimental background, the spin components of the ferromagnetic phase were investigated by the magnetic Compton scattering experiment to investigate the mechanism of the variation of magnetization.

3.5. Magnetic Compton scattering

The results of the magnetic Compton scattering performed for the ferromagnetic samples with $x = 0$, 0.1, 0.25 and 0.5 at 10 K under an applied field of 2.5 T are shown in figure 8(a). As shown in figure 8(b), the experimental profile is explained well by the calculated RHF profiles for Ru and Mn ions. In general, the width of the MCP is determined by the electron orbital radii, and the difference observed for the MCPs is caused by the difference in the spatial expanse of the Ru 4d and Mn 3d electron orbitals. Therefore, the variation

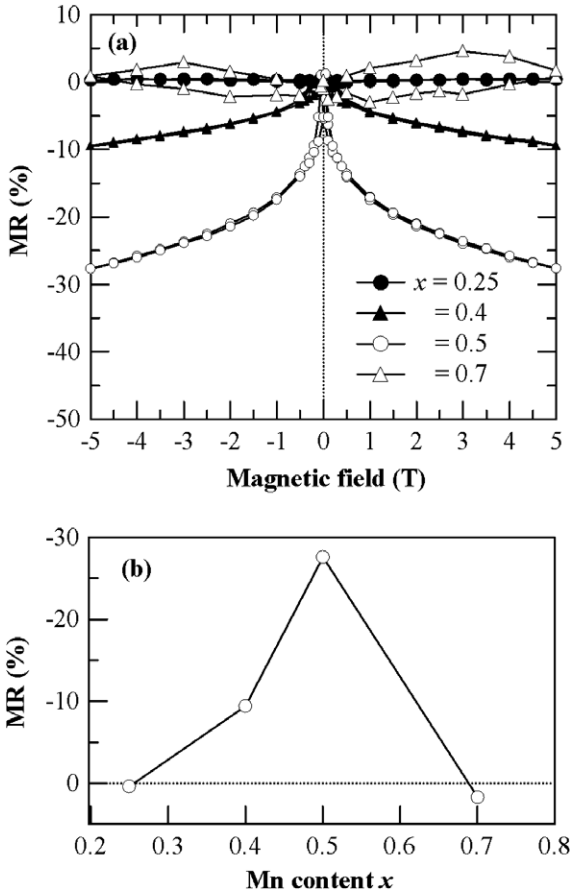

Figure 6. (a) The magnetic field dependence on MR ratio at 10 K for $Ca_{0.3}Sr_{0.7}Ru_{1-x}Mn_xO_3$. (b) The MR ratios at 5 T are plotted as a function of Mn content.

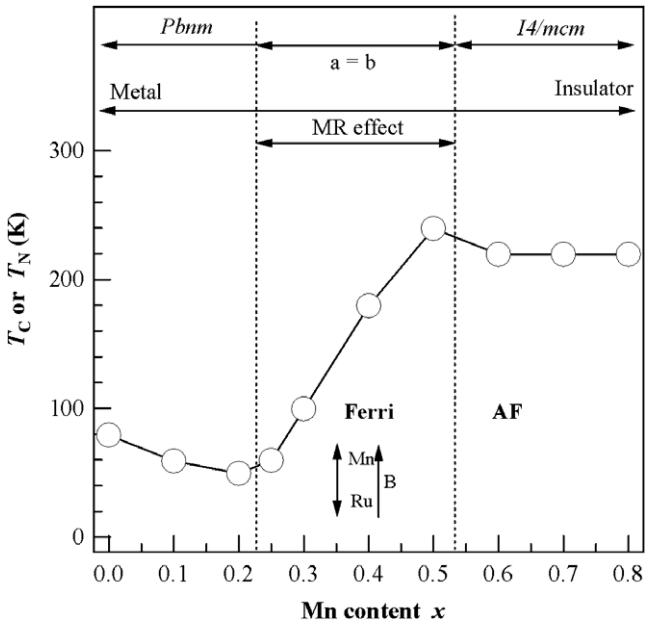

Figure 7. The electronic and magnetic phase diagram for $Sr_{0.7}Ca_{0.3}Ru_{1-x}Mn_xO_3$ system ($0 \leqslant x \leqslant 0.8$).

in MCPs suggests that the dominant magnetic component changes from Ru to Mn with increasing content of Mn in the $Ca_{0.3}Sr_{0.7}Ru_{1-x}Mn_xO_3$ system. The spin moment structure

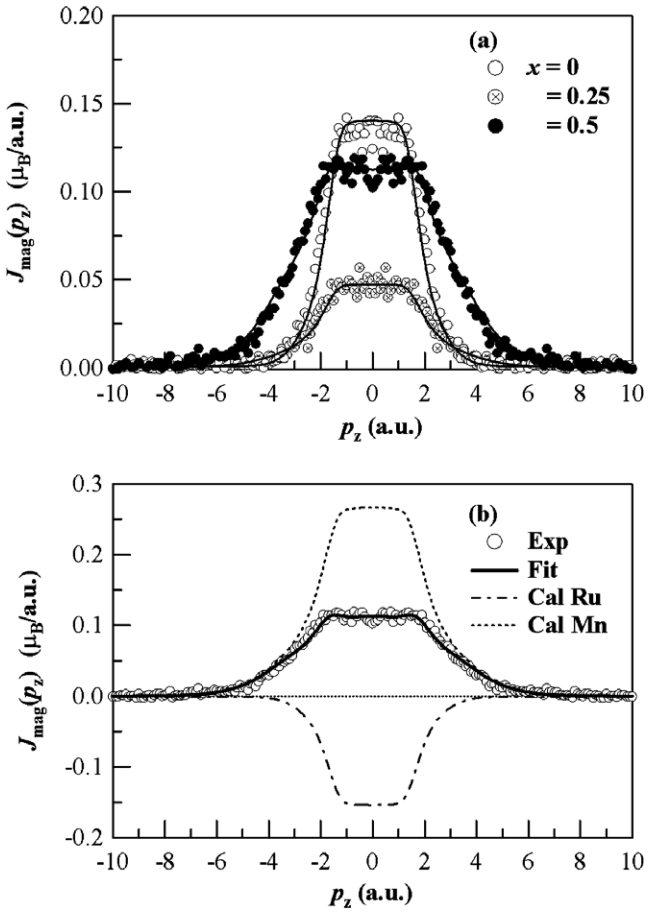

Figure 8. (a) Magnetic Compton profiles for $x = 0$, 0.25 and 0.5 from $Ca_{0.3}Sr_{0.7}Ru_{1-x}Mn_xO_3$. Experimental results were illustrated by markers along with the fitting curves based on the RHF theoretical profiles. (b) MCP shape analysis result of the sample with $x = 0.5$. The experimental MCP is represented by the combination of the calculated RHF Ru and Mn profiles.

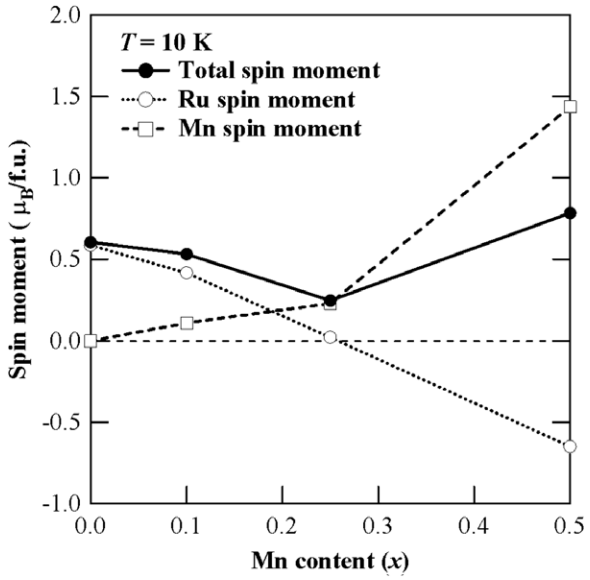

Figure 9. The variation of the total, Ru and Mn spin moments with Mn content determined from the magnetic Compton scattering experiment.

can be characterized by the curve fitting analysis of the MCP. As shown in figure 8(a), the experimental MCP for $x = 0$ agrees well with the calculated RHF profiles of Ru 4d. On the other hand, as shown in figure 8(b), the result of the analysis for $x = 0.5$ indicates that an antiferromagnetic structure of Mn and Ru moments is established in the sample. The antiferromagnetic coupling between Ru and Mn ions could be explained by the superexchange interaction via the O ion, which is similar to the $CaRu_{1-x}Mn_xO_3$ system [20, 21].

The partial spin moments were evaluated from the total spin moments and the curve fitting analysis of the magnetic Compton profile (MCP). The partial spin moments obtained for Ru and Mn ions by the MCS experiment are shown in figure 9 as a function of Mn content x. The evaluated spin moments under 2.5 T were 0.605 μ_B/f.u., 0.532 μ_B/f.u., 0.248 μ_B/f.u. and 0.784 μ_B/f.u. for $x = 0$, 0.1, 0.25 and 0.5, respectively, within the estimation error of ∼0.002 μ_B. These values agree well with those obtained by the magnetization measurement at 2.5 T and the variation of the spin moments is consistent with that of the magnetization measurement shown in figure 4. Therefore, the variation of the magnetization against Mn composition must be due to the spin moment rather than the orbital moment. The results of the MCS experiments indicate that the Mn content dependence of the magnetization (figure 3) is caused by the change in the contribution of spin components from Ru to Mn ions. The sample with $x = 0.25$, which has the minimum magnetization, must be a border composition in which the dominant magnetic component changes from Ru to Mn.

The results of the MCP analyses are summarized in figure 9. The Ru moment decreases linearly from 0.585 μ_B/f.u. for $x = 0$ to −0.65 μ_B/f.u. for $x = 0.5$ crossing 0 μ_B at $x = 0.25$, whereas the Mn moment tends to increase above $x = 0.25$ and reached 1.44 μ_B/f.u. at $x = 0.5$. The decrease in the Ru moment is described by the formula $y = 0.61–2.5x$. This result suggests that the effect of the Mn substitution on the magnetization (or spin moment) is different between the samples below and above $x = 0.25$. From this result, the mechanism of the variation in the magnetization (shown in figure 4) for ferromagnetic samples with $x < 0.5$ can be described as follows. For samples with $x < 0.25$, although the magnetic dominant is the Ru moment, it decreases as the Mn content increases due to the decrease in the amount of ferromagnetic Ru ions. Above $x = 0.25$, the ferromagnetic Mn moment becomes a magnetic dominant, and the Ru moment aligns against the direction of the Mn moment with increasing x.

4. Discussion

4.1. The MCP results and the origin of the spin moment

As shown in figure 9, it was revealed by the MCS measurements that the Mn substitution causes a variation of the total, Ru and Mn spin moments in the $Ca_{0.3}Sr_{0.7}Ru_{1-x}Mn_xO_3$ system. Here, the variation of the spin moment is discussed

based on the results of the XRD analysis, where a mixed valence state of Mn^{3+}, Mn^{4+}, Ru^{4+} and Ru^{5+} ions is assumed. The decrease in the magnetization for samples of $x < 0.25$ is caused by the decrease in the Ru moment (referred to as mechanism A). On the other hand, the increase in the magnetization for $x > 0.25$ is caused by the increase in the Mn moment (referred to as mechanism B).

In the case of mechanism A, the decrease in the Ru moment for Mn doping can be interrupted by assuming an antiparallel alignment of the ferromagnetic Ru^{4+} moment (1.3 μ_B) and the ferromagnetic Ru^{5+} moment ($S = 3/2$). The total Ru moment will be 0 μ_B at a composition $x = 0.23(=3/1.3)$, which agrees well with the composition at which minimum magnetization is observed in the magnetization measurement. Although the difference between Ru^{4+} and Ru^{5+} ions cannot be distinguished in the MCS experiment under the present experimental resolution, the variation of the Ru moment obtained from MCS experiments can be explained by using the contents of each ion, which were deduced from the XRD measurements. The XRD result indicates that the amounts of each ion in the sample with $x = 0.25$ are 0.125 for Ru^{5+}, Mn^{3+} and Mn^{4+} ions and 0.625 for the Ru^{4+} ion. In addition, the existence of an antiferromagnetic superexchange interaction between Ru^{4+} (t_{2g}) and Ru^{5+} (t_{2g}) ions has been suggested [27, 28]. Therefore, in this case, the spin moment $0.375(=0.125 \times 3)$ μ_B of Ru^{5+} and $0.375(=0.625 \times 0.6)$ μ_B of Ru^{4+} must be canceled out assuming an antiferromagnetic coupling between these ions. Moreover, the Ru moment will take a value -0.6 μ_B/f.u.$(=0.25 \times 0.6–0.25 \times 3)$ when the amounts of Ru^{4+}, Ru^{5+}, Mn^{3+} and Mn^{4+} ions equal 0.25 at $x = 0.5$.

On the other hand, in the case of mechanism B, further Mn doping over $x = 0.2$ will increase the Mn^{3+}–Mn^{4+} ferromagnetic pairs, as suggested for the $CaRu_{1-x}Mn_xO_3$ system [14, 21], and the Mn moment must then be enhanced. As reported above, the $Ca_{0.3}Sr_{0.7}Ru_{1-x}Mn_xO_3$ system is in a mixed valence state and magnetic Ru^{5+} ions exist in this system. Therefore, a ferrimagnetic cluster seems to be created by the ferromagnetic Ru^{5+}–Ru^{5+} and Mn^{3+}–Mn^{4+} pairs above $x = 0.25$, where the Ru^{4+} moment has been neglected. As a result, the increase in the magnetization for $x > 0.25$ would be induced by the increase in the amount of the ferrimagnetic cluster.

The Mn moment is tiny below $x = 0.2$ because of the small amount of the Mn^{3+}–Mn^{4+} ferromagnetic pairs and, therefore, in mechanism A, the Ru moment is the dominant magnetic component and the decrease caused in the magnetization by Mn doping is attributed to the decrease of the Ru moment. On the other hand, in mechanism B, the ferromagnetic Mn moment dominates the magnetization.

The variation of Ru and Mn moments was also pointed out for the $CaRu_{1-x}Mn_xO_3$ system [22]. However, there is a discrepancy between the present system and the $CaRu_{1-x}Mn_xO_3$ system in the amount of ferromagnetic Ru^{4+} ions in both starting materials. The discrepancy of the magnetism of the Ru^{4+} ion induced the variation of magnetization for the $Ca_{0.3}Sr_{0.7}Ru_{1-x}Mn_xO_3$ system.

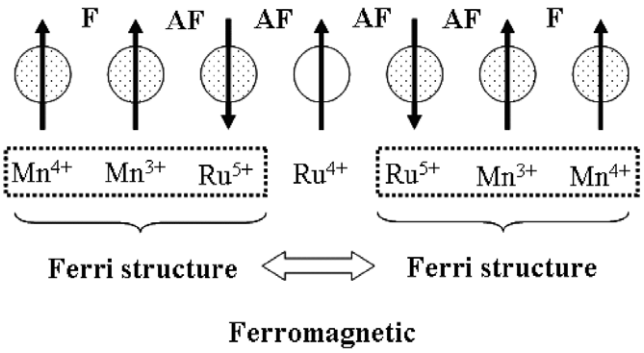

Figure 10. One of the possible atomic ordering models for the Mn^{3+}, Mn^{4+}, Ru^{4+} and Ru^{5+} ions for the sample with $x = 0.5$, which is predicted by the experimental results.

4.2. Magnetism in $Ca_{0.3}Sr_{0.7}Ru_{1-x}Mn_xO_3$ ($x < 0.25$)

The results of the MCS, resistivity and MR effect measurements can be explained assuming that the Mn substitution induces a change in the magnetism from the itinerant ferromagnetism to the localized ferromagnetism. In this assumption, an itinerant metallic component would consist of the Ru^{4+} ion and a localized component would basically consist of the Ru^{5+} ion.

From these experimental results, the transition from a metallic (itinerant) to a semiconductive (localized) state would be as follows. Very small Mn doping introduces a localized ferrimagnetic cluster, which is formed by the antiferromagnetic interaction between Mn^{3+}–Ru^{5+} ions, to the itinerant $Ca_{0.3}Sr_{0.7}RuO_3$. The increase in the Mn content would promote the binding of the localized ferrimagnetic clusters and the localized network would develop in the system of itinerant ferromagnetism as the Mn content increases. As a result, the temperature dependence of the resistivity shows a continuous change from metallic to insulating, depending on the Mn content (see figure 5). Consequently, the magnetism of the $Ca_{0.3}Sr_{0.7}Ru_{1-x}Mn_xO_3$ system ($x < 0.25$) changes, reflecting the coexistence of the Ru^{4+} and Ru^{5+} ions.

4.3. Possible magnetic structure for $Ca_{0.3}Sr_{0.7}Ru_{0.5}Mn_{0.5}O_3$

The MCS experiment revealed that the sample with $x = 0.5$ has a ferrimagnetic structure consisting of Ru and Mn moments. The magnetic spin moments assigned by the curve fitting analysis for the MCP using the spin moment ratio Mn/Ru = 2.19 are 1.44 and 0.65 μ_B/f.u. for Ru and Mn ions, respectively. On the other hand, the ion rates estimated from the results of XRD measurements provide a magnetic component ratio of Mn/Ru = 2.33 (=7/3). This value is consistent with that (Mn/Ru = 2.19) obtained by the MCS experiment, indicating that the spin moments of Mn^{3+} (4 μ_B) and Mn^{4+} (3 μ_B) ions are parallel to the applied field and the ferromagnetic spin moments of Ru^{5+} (3 μ_B) align antiparallel to the ferromagnetic Mn spin moments.

Figure 10 illustrates a possible model for the ordering of the magnetic B site ions for the sample with $x = 0.5$. In this model, ferromagnetic chains are formed by the ferrimagnetic

clusters through the Ru^{4+} ion via superexchange interaction and, therefore, the ferromagnetic region develops as the formation of a ferromagnetic chain proceeds.

This model is based on the classical superexchange interaction mechanism rules [27, 28] and the facts provided by the present study. The results of the XRD measurement indicate (1) the existence of mixed valence ionic states of Ru^{4+}, Ru^{5+}, Mn^{3+} and Mn^{4+} ions, (2) the equal rates of B site ions (see figure 2(b)) and (3) the cubic lattice structure of B site ions (see figure 2(a)). The results of the magnetic measurement indicate (4) the ferromagnetic states of B site ions (predicted from figure 4). In addition, the result of the MCS experiment indicates (5) the antiferromagnetic coupling between ferromagnetic Mn ions (or ferromagnetic Mn^{3+}–Mn^{4+} pair) and ferromagnetic Ru ions (or ferromagnetic Ru^{5+}–Ru^{5+} pair) (see figure 5(b)) and (6) the parallel alignment of Mn spin moments and antiparallel alignment of Ru^{5+} spin moments to the applied field (see the results of MCS experiments). In addition, the 180° cation–anion–cation superexchange interaction [27, 28] will provide the ordering of B site cations. For the 180° cation–O^{2-}-cation interaction, it has been suggested that the superexchange interactions among $Mn^{4+}(t_{2g}^3)$–$Ru^{5+}((t_{2g}^3))$, $Mn^{4+}(t_{2g}^3)$–$Ru^{4+}((t_{2g}^4))$ and $Ru^{5+}(t_{2g}^3)$–$Ru^{4+}((t_{2g}^4))$ are antiferromagnetic and those for $Mn^{3+}(t_{2g}^3\ e_g^1)$–$Ru^{5+}((t_{2g}^3))$ and $Mn^{3+}(t_{2g}^3\ e_g^1)$–$Ru^{4+}((t_{2g}^4))$ are ferromagnetic or antiferromagnetic depending on the difference between the p σ or p π bonds.

4.4. MR effect and J–T distortion

When the Mn content increases, the development of the ferromagnetic Mn–Ru chains causes a change in the physical properties. The development of the ferromagnetic chains appears to have a close relationship to the variation of the MR effect with the Mn content (see figures 6 and 7) because the increase in the MR effect is associated with the increase in the magnetization. The results of the MR effect suggest that the MR effect is induced by the ferromagnetic Mn^{3+}–Mn^{4+} pair.

As shown in figure 1(a), the crystal structure of the $Ca_{0.3}Sr_{0.7}Ru_{1-x}Mn_xO_3$ system changes from cubic to tetragonal as the Mn content increases, and the magnetism changes simultaneously from ferrimagnetism to ferromagnetism at this composition, as shown in figure 4(a). These results suggest the occurrence of a Jahn–Taller (JT) distortion due to Mn^{3+} ions. The JT distortion would promote the antiferromagnetic coupling between ferromagnetic chains. The antiferromagnetic coupling would be established by the antiferromagnetic coupling (t_{2g}–t_{2g}) between ferromagnetic (e_g–t_{2g}) chains along the *c* axis [27, 28]. In the ferromagnetic chain, a ferrimagnetic structure is established by the ferromagnetic Mn^{3+}–Mn^{4+} pairs and ferromagnetic Ru^{5+} ions, as shown in figure 10. These ferromagnetic Mn–Ru chains develop three-dimensionally as the Mn content increases. The JT distortion will then induce an antiferromagnetic coupling between ferromagnetic chains between the t_{2g} orbitals of Mn^{3+} ions on each chain.

5. Conclusion

The crystallographic, magnetic and electric properties of the $Ca_{0.3}Sr_{0.7}Ru_{1-x}Mn_xO_3$ system were investigated using polycrystalline samples. Through magnetic Compton scattering experiments, we found that the system has ferrimagnetism with an antiferromagnetic coupling between Ru and Mn and that the magnetic dominant changes from Ru to Mn with increasing Mn content and that the decrease in the magnetization for samples with $x < 0.25$ is induced by the decrease in the Ru moment As a result, the itinerant ferromagnetism of $Ca_{0.3}Sr_{0.7}RuO_3$ is suppressed by the Mn doping for samples with $x < 0.25$ and an Mn-based ferromagnetic order develops by forming a ferromagnetic network with the Ru ions for samples with $x \geqslant 0.25$.

Acknowledgments

The authors are very grateful to N Hiraoka (National Synchrotron Radiation Research Center, Taiwan) for his support for the experimental analysis of the magnetic Compton profile. The work conducted at Aoyama Gakuin University was supported by The Private School High-tech Research Center Program of the MEXT, Japan. The magnetic Compton scattering experiment in SPring-8 was performed with the approval of the Japan Synchrotron Radiation Research Institute (JASRI) (proposal no. 2007B1410).

References

[1] Cao G, McCall S, Shepard M and Crow J E 1997 *Phys. Rev.* B **56** 321
[2] Cao G, McCall S, Bolivar J, Shepard M, Freibert F, Henning P, Crow J E and Yuen T 1996 *Phys. Rev.* B **54** 15144
[3] Cao G, Freibert F and Crow J E 1997 *J. Appl. Phys.* **81** 3884
[4] Sugiyama T and Tsuda N 1994 *J. Phys. Soc. Japan* **63** 3798
[5] Singh R S, Medicherla V R R and Maiti K 2007 *Appl. Phys. Lett.* **91** 132503
[6] Maiti K and Singh R S 2005 *Phys. Rev.* B **71** 161102
[7] Okamoto J *et al* 2007 *Phys. Rev.* B **76** 184441
[8] Khalifah P, Ohkubo I, Christen H M and Mandrus D G 2004 *Phys. Rev.* B **70** 134426
[9] He T and Cava R J 2001 *J. Phys.: Condens. Matter* **13** 8347
[10] Sugiyama T and Tsuda N 1999 *J. Phys. Soc. Japan* **68** 1306
[11] Raveau B, Maignan A, Martin C and Hervieu M 2000 *Mater. Res. Bull.* **35** 1579
[12] Maignan A, Martin C, Hervieu M and Raveau B 2001 *Solid State Commun.* **117** 377
[13] Markovich V, Auslender M, Fita I, Puzniak R, Martin C, Wisniewski A, Maignan A, Raveau B and Gorodetsky G 2006 *Phys. Rev.* B **73** 014416
[14] Taniguchi T *et al* 2008 *Phys. Rev.* B **77** 014406
[15] Shames A I, Rozenberg E, Martin C, Maignan A, Raveau B, André G and Gorodetsky G 2004 *Phys. Rev.* B **70** 134433
[16] Terai K *et al* 2007 *J. Magn. Magn. Mater.* **310** 1070
[17] Yoshii K, Nakamura A, Mizumaki M, Tanida H, Kawamura N, Abe H, Ishii Y, Shimojo Y and Morii Y 2004 *J. Magn. Magn. Mater.* **272–276** e609

[18] Naito M, Mizusaki S, Taniguchi T, Nagata Y, Ozawa T C, Noro Y and Samata H 2008 *J. Appl. Phys.* **103** 07C906
[19] Taniguchi T *et al* 2007 *Phys. Rev.* B **75** 024414
[20] Mizusaki S, Taniguchi T, Okada N, Nagata Y, Itou M, Sakurai Y, Ozawa T C, Noro Y and Samata H 2008 *J. Appl. Phys.* **103** 07C910
[21] Mizusaki S, Taniguchi T, Okada N, Nagata Y, Hiraoka N, Itou M, Sakurai Y, Ozawa T C, Noro Y and Samata H 2009 *J. Phys.: Condens. Matter* **27** 276003
[22] Cao G, Chikara S, Elhami E, Lin X N and Schlottmann P 2005 *Phys. Rev.* B **71** 035104
[23] Yokoyama M, Satoh C, Saitou A, Kawanaka H, Bando H, Ohoyama K and Nishihara Y 2005 *J. Phys. Soc. Japan* **74** 1706
[24] Cooper M J 1985 *Rep. Prog. Phys.* **48** 415
[25] Sakai N 1998 *J. Synchrotron Radiat.* **5** 937
[26] Cooper M J, Mijnarends P E, Shiotani N, Sakai N and Bansil A 2004 *X-Ray Compton Scattering* (Oxford: Oxford University Press)
[27] Goodenough J B 2001 *Localized to Itinerant Electronic Transition in Perovskite Oxides* (New York: Springer)
[28] Goodenough J B 1966 *Magnetism and the Chemical Bond* (New York: Wiley)